Structure and Dynamics of Polyelectrolyte Surfactant Mixtures under Conditions of Surfactant Excess

Ingo Hoffmann,[1, 2, a)] Miriam Simon,[1] Bela Farago,[2] Ralf Schweins,[2] Peter Falus,[2] Olaf Holderer,[3] and Michael Gradzielski[1, b)]

[1)] *Stranski-Laboratorium für Physikalische und Theoretische Chemie,*

Institut für Chemie, Technische Universität Berlin, Straße des 17. Juni 124,

Sekr. TC 7, D-10623 Berlin, Germany

[2)] *Institut Max von Laue-Paul Langevin (ILL), 71 avenue des Martyrs, CS 20156,*

F-38042 Grenoble Cedex 9, France

[3)] *JCNS Outstation at MLZ, Forschungszentrum Jülich GmbH, Lichtenbergstr.1,*

85747 Garching, Germany

(Dated: Monday 22nd August, 2016)

Oppositely charged polyelectrolyte (PE) surfactant mixtures can self-assemble into a large variety of mesoscopic structures, so-called polyelectrolyte surfactant complexes (PESCs). These structures directly affect the macroscopic behavior of such solutions. In this study, we investigated mixtures of the cationically charged PE JR 400 and the anionic surfactant SDS with the help of different neutron scattering and fluorescence methods. While an excess of PE charges in semi dilute solutions causes an increase of viscosity, it has been observed that an excess of surfactant charges reduces the viscosity while precipitation is observed at charge equilibrium. The increase in viscosity had been investigated before and was attributed to the formation of cross links between PE chains. In this publication we focus our attention on the reduction of viscosity which is observed with an excess of surfactant charges. It is found that the PE chains form relatively large and densely packed clusters near the phase boundary on the surfactant rich side, thereby occupying less space and reducing the viscosity. For even higher surfactant concentrations, individual surfactant decorated PE chains are observed and their viscosity is found to be similar to that of the pure PE.

PACS numbers: Valid PACS appear here

Keywords: Suggested keywords

---

a)hoffmann@ill.fr

—————

b)michael.gradzielski@tu-berlin.de

I. INTRODUCTION

The peculiar self aggregation behaviour of oppositely charged polyelectrolyte (PE) surfactant mixtures has lead to quite a number of publications over the past decades[1–24]. Many different structures can be observed[6,17,25–27], which depend on various parameters of the PE, such as charge density, backbone rigidity, molecular weight or the exact location of the charge with respect to the backbone, as well as on the properties of the surfactant, such as its chain length, the type of headgroup or the number of chains in a surfactant molecule.

One of the reasons why these mixtures are commercially interesting is their ability to form complexes at very low concentrations. Typically, the cac (critical aggregation concentration) is found to be below the cmc (critical micellar concentration) by orders of magnitude[17,28,29]. Such synergistic surfactant/polyelectrolyte mixtures are for instance employed in detergency, shampoos etc[1,4,30–33].

Generally the macroscopic phase behaviour of these mixtures can be described by two monophasic regions in which clear, stable solutions are formed and a region in between where precipitation is observed. The precipitates usually form around charge equilibrium, while both an excess of surfactant or PE charges leads to the formation of stable solutions[1,16,17].

Some PE surfactant mixtures show remarkable changes in macroscopic viscosity[3,6,34–36], whereas others show hardly any changes or even a decrease[37,38]. The reason for this is not entirely clear, yet. One of the PEs which do increase the viscosity in mixtures with different surfactants quite significantly is the cationically modified hydroxyethyl cellulose JR 400[39,40]. Near the phase boundary with an excess of PE charges a very pronounced increase in viscosity is observed. If as little as 3 mM SDS (i.e., about a third of the cmc of SDS) are added to a 1 wt% solution, the viscosity increases by more than 2 orders of magnitude. This phenomenon has been attributed to the formation of mixed rodlike aggregates, which form connections between several PE chains[41–43].

Adding a little more surfactant will cause precipitation and when the precipitate is redissolved in an excess of surfactant, the viscosity drops even below the value of the pure PE solution (see fig. 1). Elucidating the mesoscopic origins for this reduction of viscosity will be the focus of this manuscript.
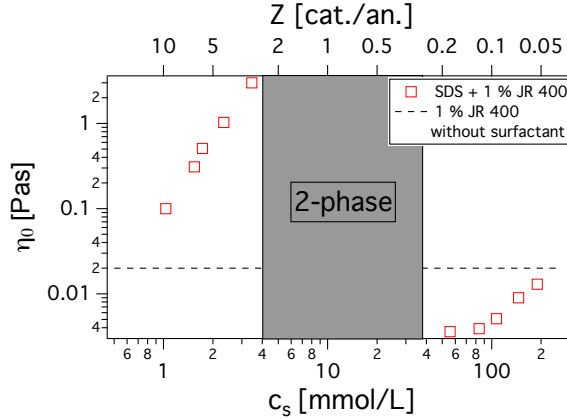
FIG. 1. Viscosity of aqueous solutions of 1 wt% JR 400 with varying amounts of SDS as a function of SDS concentration (bottom: in molar units, top: as charge ratio). The dashed line represents the viscosity of a 1 wt% JR 400 solution without added surfactant. While the viscosity is strongly increased near the phase boundary on the PE rich side of the phase diagram, the viscosity is reduced on the surfactant rich side.

II. MATERIALS AND METHODS

A. Materials

Similar to neutron scattering, fluorescence methods allow to highlight different parts of a molecule, by labeling it with specific dyes. In the experiments presented here, three different dyes were used: The PE was covalently labeled with 5-[(4,6- dichlorotriazin-2-yl)amino]fluorescein (DTAF, Sigma-Aldrich) according to the procedure described by de Belder and Granath[44] and applied previously to JR 400[30,45–47], while the hydrophobic dye Atto647 was used to specifically monitor the dynamics of the surfactant aggregates. As a reference, the diffusion of the surfactant aggregates was also investigated using another hydrophobic dye, nile red (Sigma-Aldrich).

Fluorescence correlation spectroscopy (FCS) samples were prepared by transferring a small quantity of the concentrated dye solution (nile red or Atto647 in methanol) into a vial. After the solvent was evaporated, the previously prepared aqueous solution of JR 400 and SDS was added. The dye concentration was about $5 \cdot 10^{-9}$ M in all samples.

JR 400 (Dow Chemical, USA) is a cationically modified hydroxyethylcellulose (cat-HEC) with a molecular weight of about 500000 g/mol (PDI = 1.85^{16}, partial molar density in

4

76 water 1.66 g/ml measured with an Anton Paar DMA 450 densimeter) and a cationic group

77 on 27 % of the glucose units, resulting in 1000 g of PE per mol of positive charges[48].

78 h-SDS (98.5%) and d-SDS (99.4% isotopic purity) were purchased from Sigma-Aldrich

79 and MSD Isotopes, respectively. They were used without further purification.

80 Surfactant concentrations are given as $Z = [\text{polymer charges}]/[\text{surfactant charges}]$ or as

81 molar concentrations. The PE concentration was always 1 wt% (corresponding to 10 mM

82 charges). Solutions for neutron scattering experiments were prepared in D_2O (Euriso-top,

83 France) and the JR 400 concentrations were adapted to account for the higher density of

84 D_2O. Two different contrasts were used: Full contrast with h-SDS and D_2O as solvent where

85 both the surfactant and the PE are visible and PE contrast with d-SDS and D_2O, where

86 only the PE is visible. Solutions for rheology and FCS experiments were prepared in H_2O

87 from a Millipore System.

88 ## B. Methods

89 Small angle neutron scattering (SANS) experiments were performed on the instrument

90 D11 at the Institut Laue Langevin (ILL) in Grenoble, France. Measurements were done at

91 a wavelength λ of 6 Å and for sample-to-detector distances of 1.2, 8, and 34 m to cover a

92 range of the magnitude of the scattering vector Q from 0.018 to 5 1/nm ($Q = 4\pi/\lambda \sin(\theta/2)$,

93 with scattering angle θ). Transmissions were measured with the attenuated direct beam at

94 8 m. Data reduction was performed with the software Lamp[49]. The attenuated direct beam

95 was used to obtain absolute intensities.

96 The signal obtained in SANS measurements from monodisperse, interacting objects is

97 generally given by

$$I(Q) = {}^1N P(Q) S(Q) + I_{bkg}, \tag{1}$$

99 where ${}^1N$ is the particle number density, $P(Q)$ is the form factor of the particles, which

100 accounts for intra particle scattering, $S(Q)$ is the structure factor, which accounts for inter

101 particle scattering and I_{bkg} is the incohrent background which is subtracted in all curves

102 shown here. In sufficiently dilute samples $S(Q) = 1$. The form factor is related to the scat-

103 tering amplitude $F(Q)$ by $P(Q) = F(Q)^2$ and is defined so that $P(Q = 0) = V^2(\Delta SLD)^2$,

104 where V is the volume of the particles and ΔSLD is the difference in scattering length

105 density between the particle and the matrix. ${}^1N$ is related to the volume fraction ϕ by

106    $^1N = \phi/V$.

107   If the sample is polydisperse eq. (1) takes the form

$$I(Q) = {}^1N \int_0^\infty f(R)P(Q,R)S(Q,R)\mathrm{d}R + I_{bkg}, \tag{2}$$

109 where $f(R)$ is a distribution function. The structure factor is taken into account in the

110 framework of the local monodisperse approach[50] which has been successfully used in similar

111 experiments before[51,52]. The relation between ^1N, the volume fraction, the size distribution

112 function $f(R)$ and the shape of the objects is given by

$$^1N = \frac{\phi}{\int_0^\infty f(R)V(R)\mathrm{d}R}. \tag{3}$$

114   In this paper, we used the normalized lognormal distribution function:

$$f(R, R_m, \sigma) = \frac{1}{\sqrt{2\pi}\sigma R} \exp\left(-\frac{\ln(R/R_m)^2}{2\sigma^2}\right), \tag{4}$$

116 where the mean value of the distribution is given by $M = R_m \exp(1/2\sigma^2)$ and standard

117 deviation is given by $\sqrt{\exp(\sigma^2) - 1}R_m \exp(1/2\sigma^2)$.

118   The scattering amplitude of a sphere is given by

$$F_s(Q, R, \Delta SLD) = \frac{4\pi}{3}R^3 \Delta SLD \left(3\frac{\sin(QR) - QR\cos(QR)}{(QR)^3}\right). \tag{5}$$

120   The form factor for randomly oriented core-shell rods with n shells in radial direction is

121 given by

$$P_{rod}(Q, R_{0,...,n}, \Delta SLD_{0,...,n}, L) = \left(\sum_{i=0}^n F_{rod}(Q, R_i, \Delta SLD_i, L)\right)^2, \tag{6}$$

123 with the radii of the shells R_i and the corresponding scattering length density differences

124 ΔSLD_i, where $\Delta SLD_i = SLD(R < R_i) - SLD(R > R_i)$. The thickness of a shell i is given

125 by $R_i - R_{i+1}$, where R_0 is the outer radius and R_n is the radius of the core. The scattering

126 amplitude of a rod is given by

$$F_{rod}(Q, R, \Delta SLD, L) = \pi R^2 L \, \Delta SLD \int_0^1 \frac{4J_1(Q, R\sqrt{1 - x^2})\sin(QLx/2)}{Q^2 R\sqrt{1 - x^2}Lx}\mathrm{d}x, \tag{7}$$

128   where J_1 is the first order Bessel function.

129   To describe the interactions between the charged micelles, we used the structure factor

130 for charged colloids by Baba-Ahmed, Benmouna, and Grimson[53]. It splits the interactions

6

into a contribution from an hard sphere reference fluid with an effective radius R_{eff} and a corresponding volume fraction ϕ_{eff} to account for strong repulsions at short distances and a perturbation term U_{eff}:

$$S(Q) = \frac{1}{1 - {}^1NC_{eff}(Q) - {}^1N\frac{U_{eff}(Q)}{kT}}.$$ (8)

C_{eff} is the direct correlation function of the reference hard sphere fluid, for which the Percus-Yevick approximation was used:

$$
{}^1NC_{eff}(x) = \left[A(\sin(x) - x\cos(x)) + B\left(\left(\frac{2}{x^2} - 1\right) x\cos(x) + 2\sin(x) - \frac{2}{x}\right) \right.
$$
$$
\left. - \frac{\phi_{eff}A}{2}\left(\frac{24}{(x)^3} + 4\left(1 - \frac{6}{x^2}\right)\sin(x) - \left(1 - \frac{12}{x^2} + \frac{24}{x^4}\right)x\cos(x)\right) \right] \frac{1}{x^3},
$$ (9)

where $x = 2QR_{eff}$, $A = -24\phi_{eff}\frac{(1+2\phi_{eff})^2}{(1-\phi_{eff})^4}$, $B = 36\phi_{eff}^2\frac{(2+\phi_{eff})^2}{(1-\phi_{eff})^4}$.

The pertubation term is obtained by Fourier transformation of the DLVO potential and reads

$$ {}^1NU_{eff}(x) = 24\phi_{eff}\pi\epsilon 2R_{eff}\psi^2\frac{x\cos(x) + s\sin(x)}{x^3 + xs^2}, $$ (10)

where $s = 2R_{eff}\kappa$ with the inverse Debye-Hückel screening length κ, dielectric constant ϵ and the effective surface potential

$$ \psi = \frac{le}{4\pi\epsilon R_{eff}(1 + \kappa R_{eff})}, $$ (11)

where e is the elementary charge and l is the number of charges per particle.

Neutron spin-echo (NSE) experiments were performed on the instruments IN15 (ILL) and J-NSE (MLZ) at wavelengths of 8, 10 and 12 Å (J-NSE) and 10.5 and 16 Å (IN15), respectively. Details of the experiment, the method and applications to soft matter samples are explained elsewhere[54–60]. The method yields the intermediate scattering function $S(Q,t)$, which yields an apparent diffusion coefficient D_{app} via:

$$ S(Q,t)/S(Q,0) = \exp(-D_{app}Q^2 t). $$ (12)

Rheology measurements were performed on an Anton Paar Physica MCR 501 rheometer in cone-plate geometry.

FCS measurements were performed with a Leica TCS SP5 II confocal microscope with a TCS SP5 SMD single molecule detection unit. An argon laser ($\lambda = 488$ nm) was used for

the excitation of DTAF and nile red, and a HeNe-laser ($\lambda = 633$ nm) for the excitation of Atto647. The light was delivered at the sample through an apochromatic 63x, 1.2 NA water immersion objective, the fluorescence light was collected through the same objective. The size of the confocal volume and its anisotropy have been determined before, using the dye Alexa488 with a known diffusion coefficient of 43.5 Å^2/ns.[61]

The correlation functions were obtained on a Picoharp 300 correlator and could be described with the following expression, which has proven useful for the description of anomalous diffusion or the diffusion of polydisperse samples[62–64]:

$$G(\tau) = \frac{1 + \frac{T}{1-T}\exp(-\tau/\tau_T)}{N}\left(1 + \left(\frac{4D_{app}\tau}{\omega_{x,y}^2}\right)^{\alpha}\right)^{-1}\left(1 + \left(\frac{4D_{app}\tau}{\omega_z^2}\right)^{\alpha}\right)^{-0.5}. \tag{13}$$

The first numerator accounts for the contribution from dye molecules in the triplet state, where T is the fraction of dye molecules in the triplet state and τ_T is the triplet time. This contribution can be safely neglected if either the diffusion is slow enough or the probability of the dye to be trapped in its triplet state is sufficiently low, which is the case for all dyes used here except DTAF. N is directly related to the number of dye molecules in the confocal volume, D_{app} is the apparent diffusion coefficient and ω_n is the radius of the confocal volume along the n-axis, the shape of which is assumed to be Gaussian, so that $I(n) = I_0\exp((n/2\omega_n)^2)$, with the center of the confocal volume at $n = 0$. The stretch parameter α is related to the polydispersity of the sample in analogy to the exponent in the stretched exponential function. For a monodisperse sample $\alpha = 1$. As opposed to the stretched exponential function, no analytical solution exists for the average relaxation time, therefore a numerical integration has to be performed to obtain an average diffusion coefficient:

$$D_{av} = \frac{1}{D_1}\int_0^{\infty}\left(1 + \left(\frac{4D_{app}\tau}{\omega_{x,y}^2}\right)^{\alpha}\right)^{-1}\left(1 + \left(\frac{4D_{app}\tau}{\omega_z^2}\right)^{\alpha}\right)^{-0.5}\mathrm{d}\tau, \tag{14}$$

where D_1 is the result of the integral from eq. (14) with $\alpha = 1$ and $D_{app} = 1$.

The hydrodynamic radius R_h can be calculated from the diffusion coefficient using the Stokes-Einstein equation:

$$R_h = \frac{kT}{6\pi\eta D}, \tag{15}$$

where k is Boltzmann's constant, T is the absolute temperature and η is the solvent viscosity.

Measurements with only one single dye present (DTAF or nile red) were performed using pseudo cross-correlation with a 50/50 beam splitter. Using pseudo cross-correlation has

183 the benefit to avoid artifacts from the APD detectors at short times, like the effect of
184 afterpulsing.

185 Measurements with Atto647 alone were performed with a pulsed diode laser with a wave-
186 length of 640 nm. The advantage of using a pulsed laser in this case is that it allows to
187 record a fluorescence life time signal at the same time and to reject detector counts, which
188 do not stem from fluorescence simply by limiting the number of time channels considered
189 for the calculation of the auto-correlation function.

190 Dual color cross-correlation measurements with DTAF and Atto647 have been performed
191 with an argon laser for the excitation of DTAF and a helium-neon laser for the excitation
192 of Atto647.

193 The code for the simulations was written in Python, using the package numpy.

194 All measurements were performed at 25 °C.

III.   RESULTS AND DISCUSSION

A.   SANS

197 SANS measurements were performed to elucidate the structure of the aggregates at dif-
198 ferent concentrations and under different contrast conditions.

200 From measurements in full contrast (see fig. 2), it is readily apparent, that at the lowest
201 SDS concentration 38 mM (Z = 0.26), the scattering is still dominated by rod-like aggregates
202 as can be seen from the Q^{-1} slope between 1 and 0.2 nm^{-1}, while at higher concentrations,
203 spherical charged micelles can be observed as can be seen from the emerging structure
204 factor peak. The measurements in PE contrast (see fig. 3) reveal that the PE maintains an
206 elongated conformation. The pronounced minimum at 1.3 1/nm can be ascribed to a core-
207 shell structure of the rod-like aggregates, where a surfactant core is encircled by a relatively
208 dense PE shell with a thickness of 0.7 nm. Adding more surfactant decreases the intensity
209 in PE contrast, which means that the core-shell aggregates are deteriorating. However, a
210 few of them seem to remain, as can be seen from the little kink at about 0.8 1/nm which
211 is still present at higher concentrations. Even though, the PE is no more found in rod-like
212 core-shell aggregates, it is still elongated compared to the pure PE, as can be seen from the
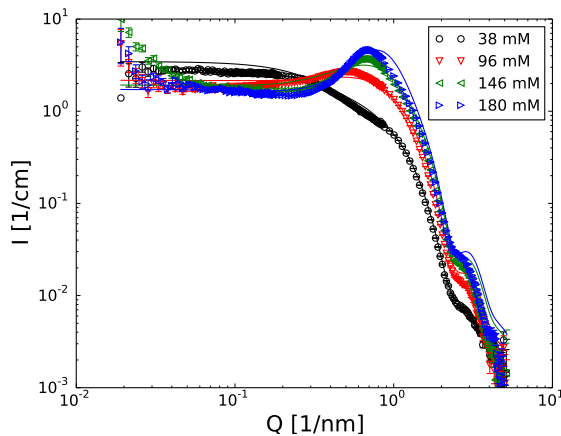213 extended Q^{-1} slope.

FIG. 2. SANS curves of h-SDS/JR 400 (1 wt%, 10 mM) mixtures at h-SDS concentrations indicated in the graph. At the lowest concentration, the scattering pattern is still dominated by mixed rodlike aggregates. At higher concentrations, the scattering curves are dominated by charged spherical micelles.
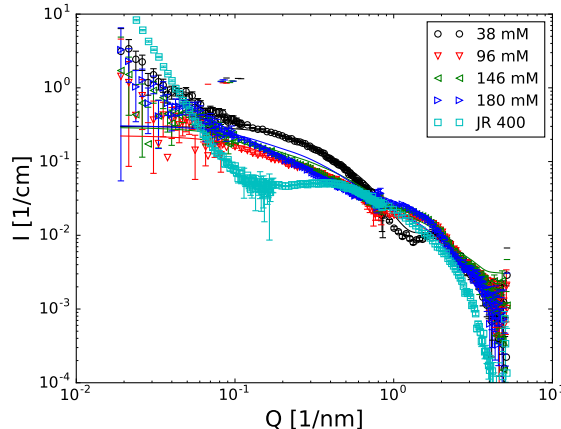

FIG. 3. SANS curves of d-SDS/JR 400 (1 wt%, 10 mM) mixtures at d-SDS concentrations indicated in the graph and pure JR 400. At the lowest concentration a significant amount of rodlike core-shell aggregates is still present. At higher concentrations, the core-shell structures disappear but the PE is still in an elongated form.

₂₁₄ Figure S1 shows the peak position in full contrast as a function of SDS concentration. If
₂₁₅ the peak is due to correlations between neighbouring adsorbed micelles along a PE chain,

216 the distance between them should scale linearly with surfactant concentration as

$$Q_{peak} = \frac{^1N}{L_{tot}}2\pi = \frac{\pi R_{pe}^2\phi}{\phi_{pe}4\pi/3R^3}2\pi, \tag{16}$$

218 where L_{tot} is the length of PE per volume, ^1N is the particle number density of the micelles,
219 ϕ is the volume fraction of the surfactant, R is the radius of the micelles, ϕ_{pe} is the volume
220 fraction of the PE and R_{pe} is the cross sectional radius of the PE chains. In deriving the
221 term after the second equality in eq. (16) it has been assumed that the micelles are spherical
222 and the cross section of the PE is circular. If the peak stems from correlations between
223 nearest neighbours of micelles in the volume phase, its position should be described by

$$Q_{peak} = \sqrt[3]{\frac{\phi}{4\pi/3R^3}}2\pi. \tag{17}$$

225 As can be seen in fig. S1 the behaviour of the peak position is reminiscent of correlations
226 in the volume phase (eq. (17)). Closer inspection reveals some slight deviations at lower
227 concentrations, which can be attributed to the fact that a signifcant amount of the surfactant
228 is still found in the rod-like aggregates at lower concentrations. This discrepancy becomes
229 smaller as more surfactant is added, meaning that the fraction of surfactant in rodlike
230 aggregates decreases at higher surfactant concentrations.

231 In order to obtain a more detailed picture of the structure of the solution the SANS
232 curves were interpreted as the combination of pure polyelectrolyte (I_{PE}), aggregates (I_{Agg})
233 and micelles (I_{mic}):

$$I(Q) = I_{PE} + I_{Agg} + I_{mic} \tag{18}$$

235 The scattering from the PE was described as a combination long and short thin rods, while
236 the aggregates are described as core shell rods with a PE shell and a surfactant core. The
237 micellar aggregates are described as charged spheres. A sketch of the model is depicted in
238 fig. S2. A more detailed description of the SANS model can be found in the supporting
239 information.

240 A summary of the parameters can be found in table S I. The results obtained for x_{sa},
241 the fraction of surfactant in the aggregates (converted to molar surfactant concentrations)
243 are shown in fig. 4. The results are in qualitative agreement with those found by comparing
244 the peak position to the results from eq. (17) and it can be seen that not only the relative
245 amount of surfactant in the rodlike aggregates decreases, as more surfactant is added but
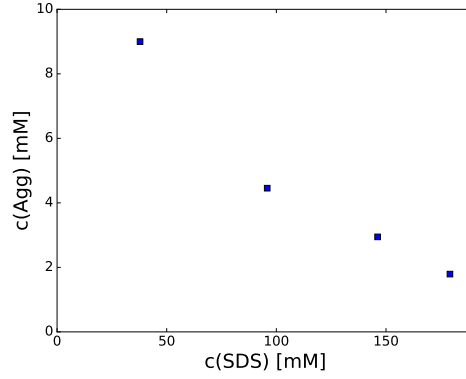
11

FIG. 4. Concentration of surfactant in rod-like aggregates as a function of total surfactant concentration obtained from fitting the SANS curves using eq. (18). The total amount of surfactant in the rodlike aggregates decreases as more surfactant is added.
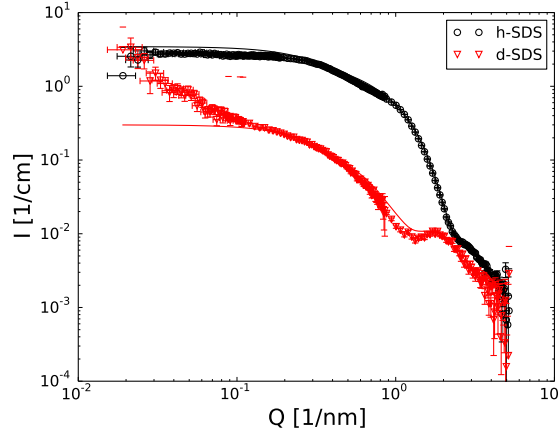

FIG. 5. SANS curves of SDS/JR 400 (1 wt%) mixtures at a SDS concentration of 38 mM, black: h-SDS, red: d-SDS, lines are fits using eq. (18). The minimum at about 1.3 1/nm can be described using a core-shell structure of the aggregates.

the total amount decreases. This means that adding more surfactant actually dissolves the rodlike surfactant/PE aggregates.

While near the phase boundary roughly a quarter of the surfactant molecules is still found in the aggregates this number decreases to less than 1% at the highest surfactant concentration.

The measurement at 38 mM SDS reveals another interesting detail. The minimum at about 1.3 1/nm in PE contrast (see figs. 3 and 5) can only be explained with a core-shell

structure of the rodlike aggregates. It is also interesting to note, that there is still some upturn in intensity towards lower Q at 38 mM SDS due to large clusters, which was also observed at PE excess. This upturn can mostly be seen using d-SDS as the clusters mostly consist of PE and the intensity from the surfactant is too high, otherwise.

A question that can not be answered satisfactorily by SANS, is whether or not the micelles are attached to the PE. While at lower concentrations, the peak position is a reliable means to differentiate between free micelles and polymer surfactant mixtures with a pearl necklace structure[19,65,66], this is not possible in more concentrated solutions such as those investigated here. At higher concentrations, the correlation peak might still occur due to correlations in the volume phase as the nearest neighbours, which are not bound to the same PE chain are still relatively close and will cause a correlation peak, even if the micelles are bound to the PE. Furthermore, it would be a somewhat surprising finding, if the oppositely charged PE would be stripped of the surfactant by adding more surfactant, which deserves independent proof from another experiment. Therefore FCS and NSE measurements were performed as the diffusion coefficients of free micelles and aggregates with bound micelles should be pronouncedly different, since they probe a dynamic property and not the static structure.

B.   FCS/NSE

While it is not possible to see from static experiments whether the micelles are free or bound, FCS should provide a clear answer as the diffusion coefficients of free micelles and PE bound micelles should be significantly different. Additionally, by using different fluorescent dyes, different parts of the system can be highlighted. Here, the hydrophobic dyes nile red (for pure SDS micelles, see fig. S5 and SDS/JR 400 aggregates) and Atto647 (for surfactant aggregates in mixtures with the PE, see fig. 6 and fig. S4 for a comparison between results obtained using Atto647 and nile red) were used to investigate the dynamics of the hydrophobic domains and DTAF was used to covalently label the PE chains (see fig. S10).

It is already clear from the diffusion coefficients obtained for pure SDS and the aggregates (see fig. 7 and figs. S6 to S9) that the micelles seen in SANS are actually bound to the PE as their diffusion is significantly slower over the whole concentration range investigated. If the PE was saturated with micelles at some concentration and free micelles started to form,
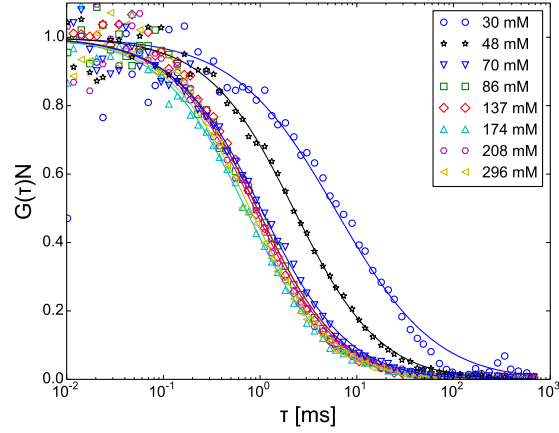
FIG. 6. Normalized correlation functions obtained with mixtures of 1 wt% JR 400 and SDS concentrations indicated in the graph. Atto647 was used as hydrophobic dye. Using a hydrophobic dye allows to monitor the dynamics of the surfactant aggregates and it can be seen that the decay becomes faster upon addition of more surfactant.
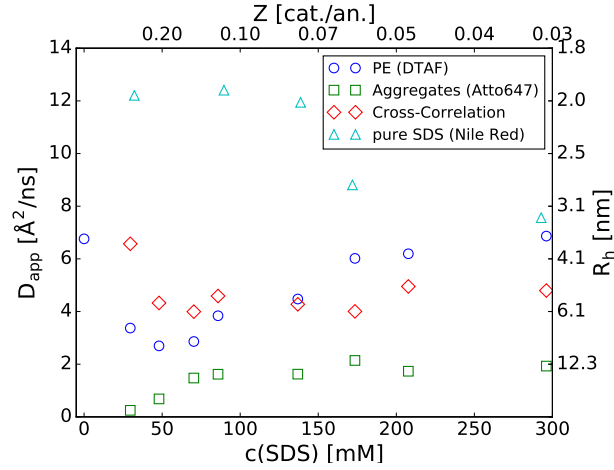

FIG. 7. D_{app} obtained from fitting eq. (13) to the FCS correlation functions. The diffusion coefficients obtained from the JR 400/SDS mixtures are significantly smaller than those of free SDS micelles, which means that there are no free micelles.

this should be reflected by an increase of D_{app} of the aggregates. However, this behaviour can not be observed and it can be concluded that the micelles are bound to the PE in the whole concentration range investigated.

The diffusion coefficient of the aggregates increases up to a surfactant concentration of about 80 mM to remain roughly constant when the surfactant concentration is further

increased (see fig. 7). It can be concluded that at this concentration, almost all of the mixed rod-like aggregates have been dissolved and what is observed is the diffusion coefficient of micelle decorated chain segments.

The dynamics of the PE chains is reflected in the diffusion coefficient obtained from measurements with covalently bound DTAF. D_{app} has a minimum at about 50 mM SDS and increases upon addition of additional SDS to reach roughly the value of pure PE at sufficiently high surfactant concentrations. The minimum can be explained when taking into account that the chain segments on which the dye label is located can either be found on a chain segment with surfactant or on a free chain segment. Adding more surfactant will decrease the fraction of free chain segments. Therefore D_{app} decreases. At the same time the diffusion coefficient of the aggregates/micelles increases as can be seen from the measurements with the hydrophobic dye Atto647. Therefore D_{app} increases and the superposition of these two effects results in a minimum.

While it should in principle be possible to differentiate between the two contributions, the diffusion coefficients seem to be a bit too close together, especially when taking into account that the decay of an FCS correlation curve is rather slow compared to e.g. DLS ($C \propto 1/\tau$ as opposed to $C \propto \exp(-\tau)$). Therefore, attempts to extract the fraction of bound PE by fitting two decays instead of one turned out to be unsuccessful. Attempting to do so is further complicated by the fact that the PE retains some of its freedom of movement in the aggregates as has been shown before[27,43] which is why taking D_{app} from the measurements with Atto647 at the same SDS concentration is not feasible and we decided to fit data with eq. (13).

Another proof of the hypothesis that the micelles observed in SANS are bound to the PE comes from the fact that the cross-correlation function obtained from cross correlating the signals from DTAF and Atto647 has a non-zero amplitude. While it should be small, as only very small fractions of the PE and the micelles are labelled (and hence, the probability for a labelled micelle to be attached to a labelled chains segment is small) it is still possible to get reasonable results (see fig. S11) and the obtained diffusion coefficients are of a similar order of magnitude as the ones obtained for the individual components.

In principle, the ratio between the amplitude of the cross-correlation function and the auto-correlation function should serve as a measure for the degree of binding between the two dyes the signals of which are being cross correlated. What is observed experimentally,
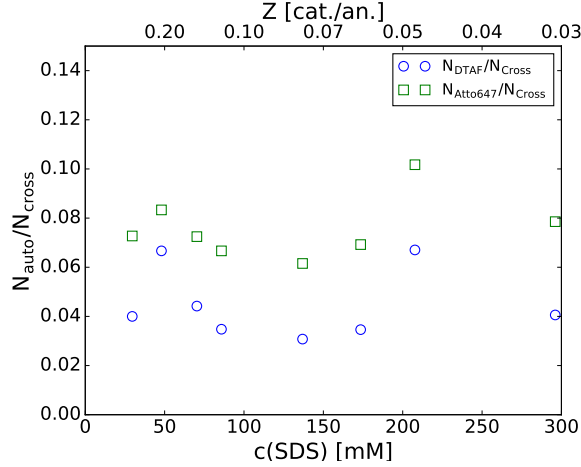
FIG. 8. Amplitudes of the cross-correlation functions relative to the amplitudes of the auto-correlation of the same experiment. The relative amplitudes remain roughly constant.

however is that the ratio remains roughly constant (see fig. 8). At first glance, this finding contradicts the idea that when adding more SDS more and more micelles are covering an increasingly large fraction of the PE, which should increase the probability for both dyes to be sufficiently close. However, in the context of FCCS (fluorescence cross-correlation spectroscopy) "sufficiently close" means that both dyes are in the confocal volume at the same time, which means that they need to be within a few 100 nm. Given the PE concentration of 1 wt% corresponds to 10 mM of charges and the average spacing between charges is about 2 nm (segments of about 0.5 nm, every 4th of them bearing a charged group) results in a total length of $2 \cdot 0.01 \, \text{nm} \cdot \text{mol/L}$ PE in all solutions. Taking a surfactant concentration of 100 mM and an aggregation number of about 100 for the micelles (corresponding to 1 mM micelles), the average spacing between micelles along the PE backbone is about $0.02 \, \text{nm} \cdot \text{mol/L} / 0.001 \, \text{mol/L} = 20 \, \text{nm}$. This is sufficiently close that wherever a DTAF group is attached to the PE backbone a micelle is close enough to contribute to the cross-correlation function if it was labelled by an Atto647 molecule and adding more surfactant does not make more DTAF groups accessible for the hydrophobic dye. Therefore the cross-correlation amplitude should remain constant.

Figure S12 compares the α parameter obtained from fitting eq. (13) to the data obtained with DTAF and Atto647. While the value of α for measurements with Atto647 is relatively low (about 0.8) for low surfactant concentrations it increases when the surfactant concentration is increased and reaches a value of 1 at surfactant concentration of about 100 mM SDS.
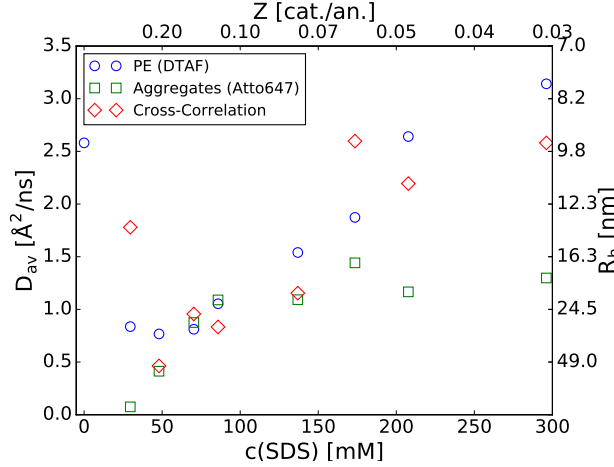
16

FIG. 9. D_{av} obtained from applying eq. (14) to the parameters obtained from fitting eq. (13) to the FCS correlation functions. The values of D_{av} for the PE and the aggregates are almost identical at sufficiently high surfactant concentrations.

344 This means that the observed dynamics stem from a relatively monodisperse population of
345 aggregates at higher surfactant concentrations, while at lower concentrations the coexistence
346 between large aggregates and micelle decorated segments in addition to the large aggregates
347 being potentially polydisperse leads to smaller values of α.

348 The α obtained with DTAF remains relatively constant over the whole concentration
349 range investigated. This may be either because there are different populations of chain
350 segments over the whole concentration range or because the diffusion of chain segments is
351 intrinsically anomalous as indicated by the finding that α has the same value even for pure
352 PE.

353 Given that α is significantly different for measurements with Atto647 and DTAF, it is
354 worthwhile to compare the average diffusion coefficient, following eq. (14), which can be
356 seen in fig. 9. While D_{app} has been found to be consistently higher for DTAF (see fig. 7)
357 this is only the case for low and high surfactant concentrations for D_{av}. For small surfactant
358 concentrations where large aggregates are still present, this can be attributed to the freedom
359 of movement of the PE chains in the aggregates. At higher surfactant concentrations, D_{av}
360 for Atto647 and DTAF have roughly the same value, which seems reasonable, as it is hard
361 to imagine what extra freedom of movement the PE should have in a volume as small as a
362 micelle.

363 At the two highest surfactant concentrations D_{av} has a higher value for DTAF again, but
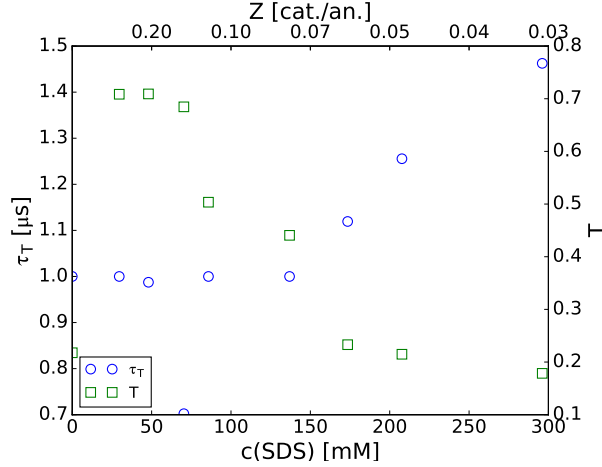
17

FIG. 10. Amplitude of the triplet contribution T and triplet time τ_T obtained from fitting eq. (13) to the FCS correlation functions of the PE. The decrease of T and increase of τ_T upon addition of surfactant show the increasingly hydrophobic environment of the dye.

this might be due to the slightly higher value of α (see fig. S12).

While the non-negligible triplet contribution for fluoresceine based dyes mostly complicates fitting the FCS data, it also has some benefits, as T and τ_T can serve as sensors for the nature of the chemical environment of the dye[67]. As can be seen in fig. 10, T decreases as more surfactant is added, which means that an increasing fraction of the dye molecules along the PE backbone are incorporated in micelles.

While FCCS measurements only show that the micelles are located within about 100 nm of a PE chain, NSE measurements (see fig. 11) show that the dynamics of both PE (measurement with d-SDS) and micelles (measurement with h-SDS) are almost identical on a nanometer length scale, which shows again that the micelles are attached to the PE. The values of D_{App} obtained for the SDS/JR 400 mixtures are smaller than the pure SDS micelles and the PE in the Q-range investigated, which means the observed dynamics stem from some segments larger than the spherical aggregates in SANS at full contrast, which is in good agreement with the extended Q^{-1} region in the corresponding SANS curves. So the diffusing subunit consists of the spherical aggregate and an extended part of the PE chain, which is apparently stiffened through the adsorption of the surfactant.
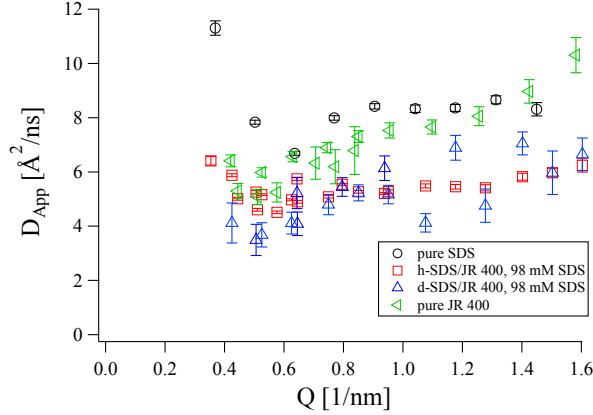
18

FIG. 11. Apparent diffusion coefficient obtained from NSE for 1wt% JR 400, SDS/JR 400 at $Z = 0.1$ with both h-SDS and d-SDS and h-SDS without JR 400 for comparison. D_{App} for d-SDS/JR 400 and h-SDS/JR 400 are almost identical and lower than both pure SDS and JR 400.

C. Simulations

From the SANS measurements, it is evident that the surfactant aggregates take the shape of small spherical micelles in the surfactant excess regime, while longer, mixed rodlike aggregates were observed in the PE excess regime. This change of shape is clearly related to the reduction in viscosity.

From these observations, two scenarios are thinkable. Either, by simply adding more surfactant to the system the relative fraction of the PE in the mixed rod-like aggregates is reduced and thereby the probability to form connections between PE chains is reduced and consequently so is the viscosity. In this scenario, the change of shape of the aggregates would merely be a side effect.

Alternatively, it is thinkable that the change of aggregate shape happens first and consequently, the smaller spherical aggregates are unable to form efficient cross links.

To shed some light on this question, we performed some simple simulations based on the same approach that was used to explain the discrepancies between DLS, NSE and rheology in mixtures of microemulsions and telechelic polymers[68].

The concept of the simulations is as follows: To a given number of elements of one species ("surfactant aggregates") a certain number of elements of a second species ("PE chains") is added. This second species has a given number of attachment points, which are randomly connected to elements of the first species. The number of attachment points of

19

the first species is not limited. Note that the choice of the "surfactant aggregates" is entirely random and does not consider any geometrical constraints. Adding more "PE chains", large interconnected clusters can be formed.

Indeed, a set of simulations with 10000 PE chains with 10 attachment points each and an increasing number of surfactant aggregates shows that beyond a certain number of surfactant aggregates the clusters are getting smaller i.e., both the number of surfactant aggregates and PE chains per cluster is reduced (fig. S13). The reduction of the number of PE chains per cluster can be considered the equivalent of a reduced viscosity. However, at the same time an increasing number of surfactant aggregates is not incorporated in the clusters, which contradicts the results from NSE and FCS, where no free micelles were observed.

Therefore, we chose to slightly alter the setup of the simulation so that the number of attachment points of the surfactant aggregates are set to a specific value while the number of attachment points of the PE chains is not limited. The total number of attachment points (the number of surfactant aggregates multiplied by the number of attachment points per surfactant aggregate) is kept constant at 10000, while the number of attachment points per surfactant aggregate is reduced, the number of PE chains was constant at 10000. The reduction of the number of attachment points per surfactant aggregates can be considered as the equivalent of the transition from larger rod like surfactant aggregates to smaller spherical micelle like structures.

The results show that the size of the clusters is reduced (lower viscosity) as the number of attachment points per surfactant aggregate is reduced (fig. 12) and by the design of the experiment, there are no free surfactant aggregates and we manage to reproduce the experimentally observed situation.

Even though, these simulations are too simplistic to draw any quantitative conclusions, on a qualitative level they suggest that the reason for the reduction of viscosity is indeed the change of shape of the surfactant aggregates which occurs when the amount of surfactant in the solution is increased and not simply the increase in the amount of surfactant, as the number of attachment points in the simulations should translate to the size of the surfactant aggregates.
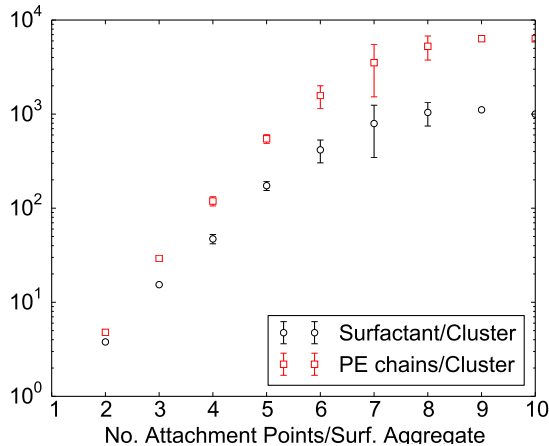
FIG. 12. Number of surfactant aggregates per cluster and number of PE chains per cluster as a function of the number of attachment points of the surfactant aggregates. The total number of attachment points was fixed at 10000 and the number of PE chains was 10000. Errorbars are the standard deviations calculated from 3 runs with the same parameters.

D. Discussion and Conclusion

By combining different methods, we have been able to shed some light on the mechanism behind the changes of the macroscopic flow behaviour in oppositely charged mixtures of the polycation JR 400 and the anionic surfactant SDS in the surfactant excess regime.

While it has been previously found that in the PE excess regime mixed rodlike aggregates are interconnecting several chains, which leads to a large increase of macroscopic viscosity through the formation of clusters[41,43], the structural origin of the behaviour in the surfactant excess regime has not been as clear so far.

The present SANS results show that rodlike aggregates are still present near the phase boundary. As opposed to the aggregates on the PE rich side of the phase diagram, these aggregates have a relatively well defined PE shell[27,43] (see fig. S3). It can be assumed, that this well defined shell is less tightly bound to the surfactant aggregates than its counter part on the PE rich side, where it was found, that the PE penetrates deeply into the aggregates. Furthermore, very low diffusion coefficients are found for the aggregates by FCS near the phase boundary on the surfactant rich side, which do not correspond to the sizes found in SANS. This means that there are large collapsed clusters of the rodlike aggregates present in the solution. Within these clusters, the PE is not likely to be able to interconnect as
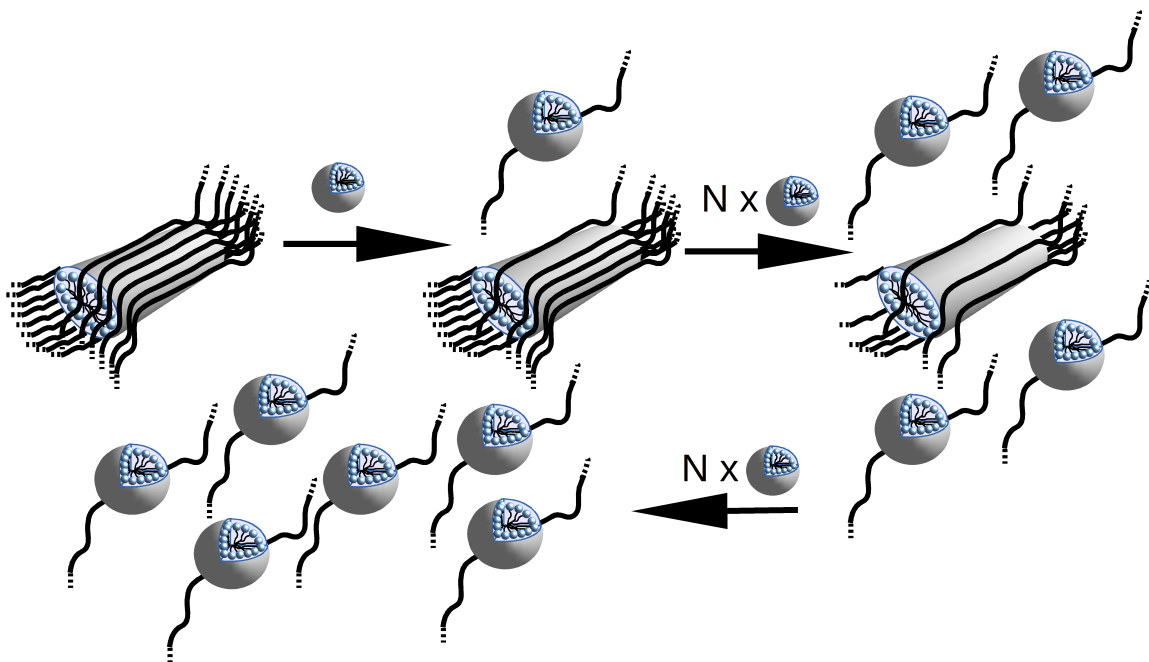
21

FIG. 13. Near the phase boundary, aggregates with a relatively dense PE shell are formed. As more surfactant is added, micelles will dissolve PE chains from the aggregates to form micelle decorated PE chains.

many different aggregates as if it was in the PE excess regime. Additionally, there may be a higher level of intra-aggregate binding of the PE chains, which results in more compact structures resulting in a viscosity even lower than that of the pure PE solution.

As more surfactant is added, the occurrence of spherical micelles is observed in SANS. At the same time the PE maintains its elongated configuration. However, the rod-like core-shell aggregates seem to become less. From the static scattering alone, it is not clear, whether the micelles are free or bound to the PE. From FCS and NSE measurements it becomes evident that they are bound to the PE, as their diffusion coefficient is too low for spherical micelles of the dimensions observed in SANS. Therefore, we can assume, that the additional micelles are dissolving PE chains from the rod-like aggregates and we are left with micelle decorated PE chains, which do not interconnect at all, but still cause an increase in viscosity by effectively occupying more volume in the solution. The sketch in fig. 13 summarizes the process described above.

SUPPLEMENTARY MATERIAL

See supplementary material for a more detailed explanation of the SANS model and additional SANS, FCS and simulation data.

ACKNOWLEDGMENTS

REFERENCES

[1] E. D. Goddard and R. B. Hannan, "Cationic polymer/anionic surfactant interactions," J. Colloid Interface Sci. **55**, 73–79 (1976).

[2] L. Piculell and B. Lindman, "Association and segregation in aqueous polymer/polymer, polymer surfactant, and surfactant surfactant mixtures - similarities and differences," Adv. Colloid Interface Sci. **41**, 149–178 (1992).

[3] U. Kästner, H. Hoffmann, R. Donges, and R. Ehrler, "Interactions between modified hydroxyethyl cellulose (hec) and surfactants," Colloids Surf., A **112**, 209–225 (1996).

[4] J. C. T. Kwak, ed., *Polymer-Surfactant Systems*, Vol. 77 (Marcel Dekker, Inc., 1998).

[5] S. Kosmella, J. Kötz, K. Shirahama, and J. Liu, "Cooperative nature of complex formation in mixed polyelectrolyte-surfactant systems," J. Phys. Chem. B **102**, 6459–6464 (1998).

[6] E. F. Marques, O. Regev, A. Khan, M. D. G. Miguel, and B. Lindman, "Interactions between catanionic vesicles and oppositely charged polyelectrolytes phase behavior and phase structures," Macromolecules **32**, 6626–6637 (1999).

[7] M. Tsianou, A. L. Kjøniksen, K. Thuresson, and B. Nyström, "Light scattering and viscoelasticity in aqueous mixtures of oppositely charged and hydrophobically modified polyelectrolytes," Macromolecules **32**, 2974–2982 (1999).

[8] Y. Yamaguchi, Y. Inaba, H. Uchiyama, and H. Kunieda, "Anomalous phase behavior of water-soluble polyelectrolyte and oppositely charged surfactants," Colloid Polym. Sci. **277**, 1117–1124 (1999).

[487] [9]A. Svensson, J. Sjöström, T. Scheel, and L. Piculell, "Phases and structures of a polyion-[488] surfactant ion complex salt in aqueous mixtures: cationic hydroxyethyl cellulose with [489] dodecylsulfate counterions," Colloids Surf., A **228**, 91–106 (2003).

[490] [10]S. Trabelsi, S. Guillot, E. Raspaud, M. Delsanti, D. Langevin, and F. Boué, "New nano-[491] and microparticles with a liquid-crystal-like interior," Adv. Mater. **18**, 2403–2406 (2006).

[492] [11]S. Dos Santos, C. Gustavsson, C. Gudmundsson, P. Linse, and L. Piculell, "When do [493] water-insoluble polyion - surfactant ion complex salts "redissolve" by added excess surfac-[494] tant?" Langmuir **27**, 592–603 (2010).

[495] [12]V. D. Lam and L. M. Walker, "A ph-induced transition of surfactant-polyelectrolyte ag-[496] gregates from cylindrical to string-of-pearls structure," Langmuir **26**, 10489–10496 (2010).

[497] [13]E. K. Penott-Chang, M. Ruppel, D. V. Pergushov, A. B. Zezin, and A. H. Müller, [498] "Interpolyelectrolyte complexes of diblock copolymers via interaction of complementary [499] polyelectrolyte-surfactant complexes in chloroform," Polymer **52**, 4296–4302 (2011).

[500] [14]E. Moroz, J. Zakharova, V. Sergeyev, and A. Zezin, "Ternary complexes polyelectrolyte-[501] oppositely charged surfactant-carbon nanotubes: Formation and properties," Dokl. Phys. [502] Chem. **441**, 212–214 (2011).

[503] [15]M. Štěpánek, J. Škvarla, M. Uchman, K. Procházka, B. Angelov, L. Kováčik, V. M. [504] Garamus, C. Mantzaridis, and S. Pispas, "Wormlike core-shell nanoparticles formed by [505] co-assembly of double hydrophilic block polyelectrolyte with oppositely charged fluorosur-[506] factant," Soft Matter **8**, 9412–9417 (2012).

[507] [16]D. Li, M. S. Kelkar, and N. J. Wagner, "Phase behavior and molecular thermodynamics of [508] coacervation in oppositely charged polyelectrolyte/surfactant systems: A cationic polymer [509] jr 400 and anionic surfactant sds mixture," Langmuir **28**, 10348–10362 (2012).

[510] [17]L. Chiappisi, I. Hoffmann, and M. Gradzielski, "Complexes of oppositely charged poly-[511] electrolytes and surfactants - recent developments in the field of biologically derived poly-[512] electrolytes," Soft Matter **9**, 3896–3909 (2013).

[513] [18]L. Chiappisi, D. Li, N. J. Wagner, and M. Gradzielski, "An improved method for analyzing [514] isothermal titration calorimetry data from oppositely charged surfactant polyelectrolyte [515] mixtures," J. Chem. Thermodynamics **68**, 48–52 (2014).

[516] [19]L. Chiappisi, S. Prevost, and M. Gradzielski, "Form factor of cylindrical superstructures [517] composed of globular particles," J. Appl. Crystallogr. **47**, 827–834 (2014).

[20] R. A. Campbell, M. Yanez Arteta, A. Angus-Smyth, T. Nylander, B. A. Noskov, and I. Varga, "Direct impact of nonequilibrium aggregates on the structure and morphology of pdadmac/sds layers at the air/water interface," Langmuir **30**, 8664–8674 (2014).

[21] L. Chiappisi, S. Prévost, I. Grillo, and M. Gradzielski, "From crab shells to smart systems: Chitosan-alkylethoxy carboxylate complexes," Langmuir **30**, 10608–10616 (2014).

[22] I. Hoffmann, "Neutrons for the study of dynamics in soft matter systems," Colloid Polym. Sci. **292**, 2053–2069 (2014).

[23] E. Fegyver and R. Meszaros, "The impact of nonionic surfactant additives on the nonequilibrium association between oppositely charged polyelectrolytes and ionic surfactants," Soft Matter **10**, 1953–1962 (2014).

[24] L. Chiappisi, M. Simon, and M. Gradzielski, "Toward bioderived intelligent nanocarriers for controlled pollutant recovery and ph-sensitive binding," ACS Appl. Mater. Interfaces **7**, 6139–6145 (2015).

[25] I. Hoffmann, P. Heunemann, B. Farago, I. Grillo, O. Holderer, M. Päch, and M. Gradzielski, "Structure and dynamics of nanoemulsions: Insights from combining dynamic and static neutron scattering," Phys. Rev. E **86**, 061407 (2012).

[26] L. Chiappisi, S. Prevost, I. Grillo, and M. Gradzielski, "Chitosan/alkylethoxy carboxylates: A surprising variety of structures," Langmuir **30**, 1778–1787 (2014).

[27] I. Hoffmann, B. Farago, R. Schweins, P. Falus, M. Sharp, S. Prévost, and M. Gradzielski, "On the mesoscopic origins of high viscosities in some polyelectrolyte-surfactant mixtures," J. Chem. Phys. **143**, 074902 (2015).

[28] K. Ohbu, O. Hiraishi, and I. Kashiwa, "Effect of quaternary ammonium substitution of hydroxyethylcellulose on binding of dodecyl sulfate," J. Am. Oil Chemists' Soc. **59**, 108–112 (1982).

[29] Y. Lapitsky, M. Parikh, and E. W. Kaler, "Calorimetric determination of surfactant/polyelectrolyte binding isotherms," J. Phys. Chem. B **111**, 8379–8387 (2007).

[30] S. T. A. Regismond, Y.-M. Heng, E. D. Goddard, and F. M. Winnik, "Fluorescence microscopy observation of the adsorption onto hair of a fluorescently labeled cationic cellulose ether," Langmuir **15**, 3007–3010 (1999).

[31] C. D. Bain, P. M. Claesson, D. Langevin, R. Meszaros, T. Nylander, C. Stubenrauch, S. Titmuss, and R. von Klitzing, "Complexes of surfactants with oppositely charged polymers at surfaces and in bulk," Adv. Colloid Interface Sci. **155**, 32–49 (2010).

[32] A. Mohr, T. Nylander, L. Piculell, B. Lindman, V. Boyko, F. W. Bartels, Y. Liu, and V. Kurkal-Siebert, "Mixtures of cationic copolymers and oppositely charged surfactants: Effect of polymer charge density and ionic strength on the adsorption behavior at the silica-aqueous interfaces," ACS Appl. Mater. Interfaces **4**, 1500–1511 (2012).

[33] J. S. Weston, J. H. Harwell, B. J. Shiau, and M. Kabir, "Disrupting admicelle formation and preventing surfactant adsorption on metal oxide surfaces using sacrificial polyelectrolytes." Langmuir **30**, 6384–8 (2014).

[34] L. G. Patruyo, A. J. Müller, and A. E. Sáez, "Shear and extensional rheology of solutions of modified hydroxyethyl celluloses and sodium dodecyl sulfate," Polymer **43**, 6481–6493 (2002).

[35] B. Nyström, A.-L. Kjøniksen, N. Beheshti, K. Zhu, and K. D. Knudsen, "Rheological and structural aspects on association of hydrophobically modified polysaccharides," Soft Matter **5**, 1328–1339 (2009).

[36] N. Beheshti, A.-L. Kjøniksen, K. Zhu, K. D. Knudsen, and B. Nyström, "Viscosification in polymer-surfactant mixtures at low temperatures," J. Phys. Chem. B **114**, 6273–6280 (2010).

[37] S. Guillot, D. McLoughlin, N. Jain, M. Delsanti, and D. Langevin, "Polyelectrolyte-surfactant complexes at interfaces and in bulk," J. Phys.: Condens. Matter **15**, S219–S224 (2003).

[38] N. Jain, S. Trabelsi, S. Guillot, D. McLoughlin, D. Langevin, P. Letellier, and M. Turmine, "Critical aggregation concentration in mixed solutions of anionic polyelectrolytes and cationic surfactants," Langmuir **20**, 8496–8503 (2004).

[39] M. Tsianou and P. Alexandridis, "Control of the rheological properties in solutions of a polyelectrolyte and an oppositely charged surfactant by the addition of cyclodextrins," Langmuir **15**, 8105–8112 (1999).

[40] I. S. Chronakis and P. Alexandridis, "Rheological properties of oppositely charged polyelectrolyte?surfactant mixtures:? effect of polymer molecular weight and surfactant architecture," Macromolecules **34**, 5005–5018 (2001).

[41] I. Hoffmann, P. Heunemann, S. Prévost, R. Schweins, N. J. Wagner, and M. Gradzielski, "Self-aggregation of mixtures of oppositely charged polyelectrolytes and surfactants studied by rheology, dynamic light scattering and small-angle neutron scattering," Langmuir **27**, 4386–4396 (2011).

[582] [42] I. Hoffmann, S. Prévost, M. Medebach, S. E. Rogers, N. J. Wagner, and M. Gradzielski, "Control of rheological behaviour with oppositely charged polyelectrolyte surfactant mixtures," Tenside, Surfactants, Deterg. **48**, 488–494 (2011).

[585] [43] I. Hoffmann, B. Farago, R. Schweins, P. Falus, M. Sharp, and M. Gradzielski, "Structure and dynamics of polyelectrolytes in viscous polyelectrolyte-surfactant complexes at the mesoscale," Europhys. Lett. **104**, 28001 (2013).

[588] [44] A. N. de Belder and K. Granath, "Preparation and properties of fluorescein-labelled dextrans," Carbohydr. Res. **30**, 375–378 (1973).

[590] [45] F. M. Winnik and S. T. Regismond, "Fluorescence methods in the study of the interactions of surfactants with polymers," Colloids Surf., A **118**, 1–39 (1996).

[592] [46] I. Hoffmann, C. Oppel, U. Gernert, P. Barreleiro, W. von Rybinski, and M. Gradzielski, "Adsorption isotherms of cellulose-based polymers onto cotton fibers determined by means of a direct method of fluorescence spectroscopy," Langmuir **28**, 7695–7703 (2012).

[595] [47] I. Hoffmann, M. Theile, S. Grätz, J. Scholz, P. Barreleiro, W. von Rybinski, and M. Gradzielski, "On the influence of surfactants on the adsorption of polysaccharide-based polymers on cotton studied by means of fluorescence spectroscopy," Langmuir **28**, 11400–11409 (2012).

[599] [48] K. Thuresson, S. Nilsson, and B. Lindman, "Effect of hydrophobic modification on phase behavior and rheology in mixtures of oppositely charged polyelectrolytes," Langmuir **12**, 530–537 (1996).

[602] [49] "LAMP, the Large Array Manipulation Program. http://www.ill.eu/data_treat/lamp/the-lamp-book/ ," .

[604] [50] J. S. Pedersen, "Determination of size distribution from small-angle scattering data for systems with effective hard-sphere interactions," J. Appl. Crystallogr. **27**, 595–608 (1994).

[606] [51] T. Foster, T. Sottmann, R. Schweins, and R. Strey, "Small-angle neutron scattering from giant water-in-oil microemulsion droplets. i. ternary system," J. Chem. Phys. **128**, 054502–13 (2008).

[609] [52] T. Foster, T. Sottmann, R. Schweins, and R. Strey, "Small-angle-neutron-scattering from giant water-in-oil microemulsion droplets. ii. polymer-decorated droplets in a quaternary system," J. Chem. Phys. **128**, 064902–18 (2008).

[612] [53] L. Baba-Ahmed, M. Benmouna, and M. J. Grimson, "Elastic scattering from charged colloidal dispersions," Phys. Chem. Liq. **16**, 235–238 (1987).

[54] P. Schleger, B. Alefeld, J. Barthelemy, G. Ehlers, B. Farago, P. Giraud, C. Hayes, A. Kollmar, C. Lartigue, F. Mezei, and D. Richter, "The long-wavelength neutron spin-echo spectrometer in15 at the institut laue-langevin," Phys. B **241–243**, 164–165 (1997).

[55] F. Mezei, "Neutron spin echo," in *Lecture Notes in Physics*, Vol. 128, edited by F. Mezei (Springer Berlin / Heidelberg, 1980) pp. 1–26.

[56] D. Richter, M. Monkenbusch, A. Arbe, and J. Colmenero, "Neutron spin echo in polymer systems," Adv. Polym. Sci. **174**, 1–221 (2005).

[57] O. Holderer, M. Monkenbusch, R. Schätzler, H. Kleines, W. Westerhausen, and D. Richter, "The jcns neutron spin-echo spectrometer j-nse at the frm ii," Measurement Sci. Technology **19**, 034022– (2008).

[58] B. Farago, "Recent developments and applications of nse in soft matter," Curr. Opin. Colloid Interface Sci. **14**, 391–395 (2009).

[59] J. Colmenero and A. Arbe, "Recent progress on polymer dynamics by neutron scattering: From simple polymers to complex materials," J. Polym. Sci. Part B: Polym. Phys. **51**, 87–113 (2013).

[60] B. Farago, P. Falus, I. Hoffmann, M. Gradzielski, F. Thomas, and C. Gomez, "The in15 upgrade," Neutron News **26**, 15–17 (2015).

[61] Z. Petrášek and P. Schwille, "Precise measurement of diffusion coefficients using scanning fluorescence correlation spectroscopy," Biophys. J. **94**, 1437–1448 (2008).

[62] P. Malo de Molina, M.-S. Appavou, and M. Gradzielski, "Oil-in-water microemulsion droplets of tdmao/decane interconnected by the telechelic c18-eo150-c18: clustering and network formation," Soft Matter **10**, 5072–5084 (2014).

[63] D. S. Banks and C. Fradin, "Anomalous diffusion of proteins due to molecular crowding," Biophys. J. **89**, 2960–2971 (2005).

[64] M. Weiss, M. Elsner, F. Kartberg, and T. Nilsson, "Anomalous subdiffusion is a measure for cytoplasmic crowding in living cells," Biophys. J. **87**, 3518–3524 (2004).

[65] B. Cabane, "Structure of some polymer detergent aggregates in water," J. Phys. Chem. **81**, 1639–1645 (1977).

[66] R. Schweins and K. Huber, "Particle scattering factor of pearl necklace chains," Macromol. Symp. **211**, 25–42 (2004).

[67] J. Widengren, U. Mets, and R. Rigler, "Fluorescence correlation spectroscopy of triplet states in solution: a theoretical and experimental study," J. Phys. Chem. **99**, 13368–13379

646   (1995).

647   [68]I. Hoffmann, P. Malo de Molina, B. Farago, P. Falus, C. Herfurth, A. Laschewsky, and

648   M. Gradzielski, "Dynamics of microemulsions bridged with hydrophobically end-capped

649   star polymers studied by neutron spin-echo," J. Chem. Phys. **140**, 034902 (2014).

Legend (within figure):
- Surfactant/Cluster (○)
- PE chains/Cluster (□)

Axis labels:
- y-axis: 10^0, 10^1, 10^2, 10^3, 10^4
- x-axis: No. Attachment Points/Surf. Aggregate (1 through 10)